

# Theoretical analysis on the stability of 1-pyrenebutanoic acid, succinimidyl ester adsorbed on graphene

Yasuhiro Oishi,<sup>\*,†</sup> Hirotsugu Ogi,<sup>‡</sup> Satoshi Hagiwara,<sup>¶</sup> Minoru Otani,<sup>¶</sup> and  
Koichi Kusakabe<sup>§</sup>

<sup>†</sup>*Graduate School of Engineering Science, Osaka University, 1-3 Machikaneyama-cho,  
Toyonaka, Osaka 560-8531, Japan*

<sup>‡</sup>*Graduate School of Engineering, Osaka University, Suita, Osaka 565-0871, Japan*

<sup>¶</sup>*Center for Computational Sciences, University of Tsukuba, 1-1-1, Tenno-dai, Tsukuba,  
Ibaraki 305-8577, Japan*

<sup>§</sup>*Graduate School of Science, University of Hyogo, 3-2-1 Koto, Kamigori-cho, Ako, Hyogo  
678-1297, Japan*

E-mail: ooishi.y@opt.mp.es.osaka-u.ac.jp

## Abstract

In this study, the adsorbed structure of 1-pyrenebutanoic acid, succinimidyl ester (PASE) on graphene was theoretically investigated based on density functional theory (DFT). We found two locally stable structures: a straight structure with the chain-like part of butanoic acid succinimidyl ester (BSE) lying down and a bent structure with the BSE part directing away from the graphene surface keeping the pyrene (Py) part adsorbed on graphene. We estimated the contribution of each part, *i.e.*, the Py and BSE parts, to the entire PASE adsorption to elucidate the adsorption mechanism. The

BSE contribution to the entire adsorption was found to be nonnegligible compared with that of Py; however, the adsorption effect of the BSE part was secondary. Kinematics analysis demonstrates that the direction of the BSE part can easily change at the room temperature. Considering the hydration effect on the PASE molecule, we applied a three dimensional reference interaction site model. The solvent environment was found to contribute to the stabilization of the bent PASE structure relative to the straight PASE structure. In a DFT simulation including glycines, the contribution to stabilizing the bent PASE structure was also found. Therefore, the effect of external environment around PASE is of importance when the standing up process of the BSE part from the graphene surface is considered.

## Introduction

Graphene, a single-atom-thick and two-dimensional carbon material, has attracted considerable application attention for biosensing devices.<sup>1-7</sup> Owing to its excellent characteristics, such as wide detection area, high carrier mobility, and large heat conductance,<sup>8,9</sup> graphene is an ideal candidate for biosensor substrates.<sup>7</sup>

Important nature in the performance is achieved by functionalization of the graphene surface with receptors such as antibodies. Covalent functionalization of graphene is a common approach.<sup>10</sup> However, this approach may cause a significant change in the electronic properties of graphene,<sup>3</sup> degrading the performance. Meanwhile, noncovalent functionalization of graphene, which employs  $\pi$ - $\pi$  stacking, can preserve electronic properties.<sup>11-13</sup> In the noncovalent approach, the graphene surface and target proteins are connected via linker molecules.

A commonly used linker molecules is 1-pyrenebutanoic acid, succinimidyl ester (PASE), which comprises the pyrene (Py) and chain-like parts made of butanoic acid succinimidyl ester (BSE), as shown in Figure 1. The succinimide group in BSE part reacts with amines in protein by forming an amide bond, whereas the Py part is considered to noncovalently bind

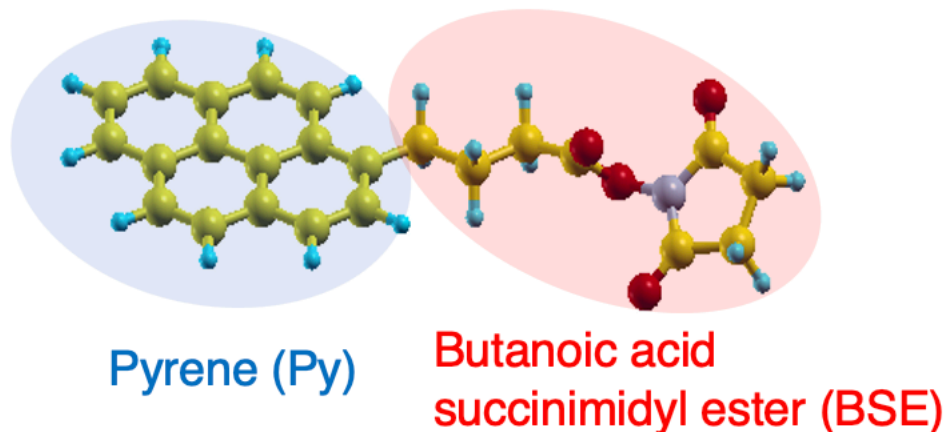


Figure 1: The structure of 1-pyrenebutanoic acid succinimidyl ester (PASE). Atomic geometries are visualized by Xcrysden<sup>14</sup> in this study (yellow: C, blue: H, red: O, and gray: N).

to graphitic materials via  $\pi$ - $\pi$  stacking.<sup>15-18</sup> Actually, PASE linkers are also used on phonon biosensor using graphene. The direct determination of phonon velocities in substrate materials affected by adsorbates is sufficiently sensitive to detect adsorbed biomaterials. Recently, based on this mechanism, biosensing graphene device has been fabricated using the picosecond ultrasonic spectroscopy method.<sup>19,20</sup> For measurement analysis, the detailed adsorption mechanism for the adsorbates, including linker molecules, should be elucidated. Because the vibrational properties of this system are significantly affected by microscopic material structures, we should determine the adsorbed conformation of linkers. Understanding the adsorption mechanism of PASE on graphene allows us to improve the biosensing device.

The adsorption of PASE on graphitic materials is determined by the Py adsorption mechanism on graphene; the Py adsorption mainly comes from the van der Waals interaction stabilizing the  $\pi$ - $\pi$  stacking.<sup>21</sup> On the other hand, BSE part is often assumed to be the site where the protein binds. This naturally makes us assume the conformation of PASE that the BSE part is standing up from graphene,<sup>11,15</sup> which we call the standing conformation. However, the standing conformation might not be always the case. In other words, the standing conformation might appear only when the graphene-PASE adsorption and protein-PASE bindings are simultaneously formed. Actually, in another linker—1-pyrenebutyric

acid—larger binding energy was found when the butyric acid side group was bonded to the graphene sheet ( $-1.54$  eV) than another case when the butyric acid chain was directed away from the graphene surface ( $-1.30$  eV).<sup>22</sup> Therefore, the adsorption of the PASE linker should, similarly, be due to two contributions of adsorption energies, *i.e.*, from Py and BSE, thereby requiring us to consider the straight PASE structure, in which both the Py and BSE parts are lying flat on the graphene surface.

In this study, we theoretically explored the stability of the PASE/graphene system. The structural optimization was performed with density functional theory (DFT). We found two locally stable structures: conformation 1, where the BSE part is lying down, and conformation 2, where the BSE part is standing up. To consider the influence of the solvent on the PASE/graphene system stability, we evaluated the total energies of conformations 1 and 2 using DFT coupled with a three dimensional reference interaction site model (3D-RISM).<sup>23,24</sup> We also considered the existence of amino acids around PASE linker by including glycine molecules in our DFT simulation. The structural optimization of the system where glycine molecules are placed around PASE adsorbed on graphene were performed.

## Results and discussion

### Adsorption structure and energy

We performed the full structural optimization on the standing conformation of PASE, where the BSE part is spatially separated from and the Py part is lying flat on the graphene surface (conformation 2). However, because the partly planer BSE part can show a nonnegligible contribution to stabilizing an adsorbed structure on graphene, there can be adsorption energy caused due to BSE on graphene. Therefore, the straight PASE structure, where not only the Py part but also the chain-like BSE part is lying down on graphene (conformation 1), was also considered. Figure 2(a) and (b) show the optimized structures for conformation 1 and 2, respectively. Conformation 3, where the BSE part is lying down and the Py part is

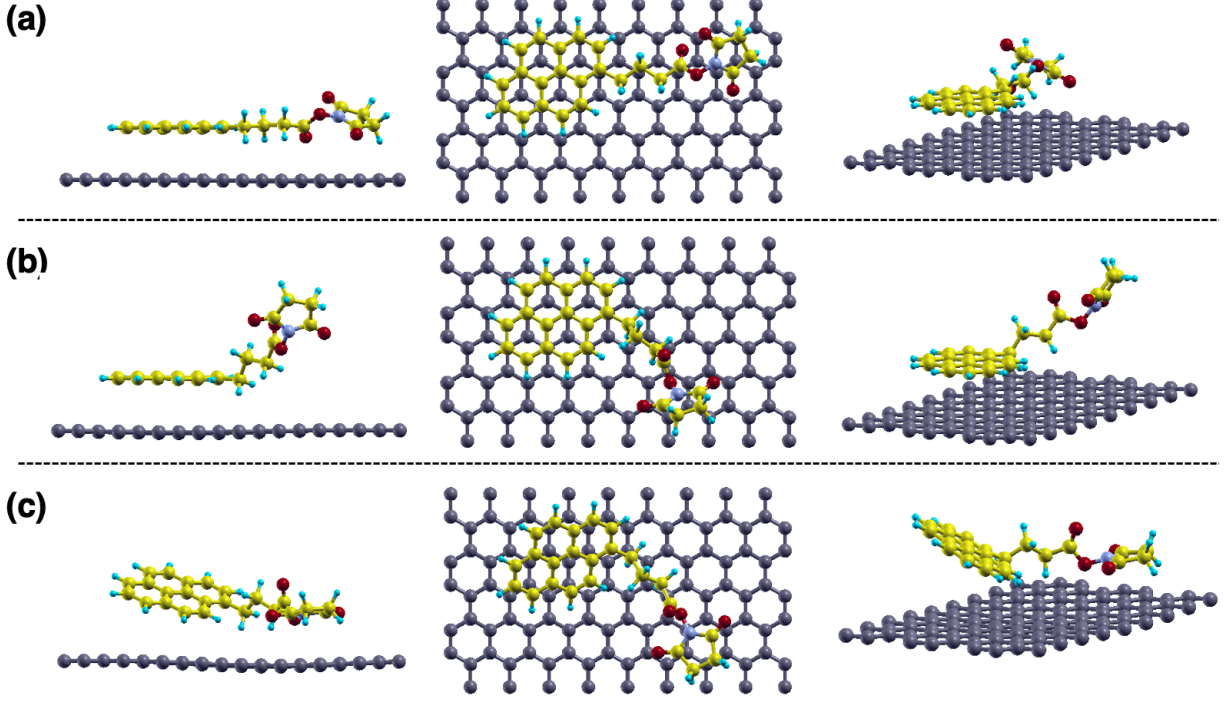


Figure 2: (a)–(c) The optimized PASE structure of conformation 1–3, respectively.

directing away from graphene, was also considered as a reference, as shown in Figure 2(c). In the structural optimization of conformation 3, the tilted structure of the Py group was fixed (only the structures of graphene and BSE part of PASE were relaxed).

For each PASE conformation, the adsorption energy was calculated. The adsorption energy  $E_{\text{ad}}^{(\text{conf}-i)}$  of conformation  $i$  ( $i = 1, 2, 3$ ) was calculated as follows:

$$E_{\text{ad}}^{(\text{conf}-i)} = E_{\text{PASE}} + E_{\text{graphene}} - E_{\text{PASE/graphene}}$$

where  $E_{\text{PASE}}$  and  $E_{\text{graphene}}$  denote the total energies of isolated PASE and graphene, respectively;  $E_{\text{PASE/graphene}}$  is the total energy of the PASE/graphene system. From the definition of  $E_{\text{ad}}^{(\text{conf}-i)}$ , a positive value is exothermic. The adsorption energies of each PASE conformation are summarized in Table 1.

The adsorption energy of conformation 1 was larger than that of conformation 2 ( $E_{\text{ad}}^{(\text{conf}-1)} >$

Table 1: Adsorption energy of each PASE conformation  $E_{\text{ad}}^{(\text{conf}-i)}$  ( $i = 1, 2, 3$ ) and pyrene  $E_{\text{ad}}^{(\text{Py})}$ .

Adsorbate	Adsorption energy (eV)
PASE conformation 1	1.63
PASE conformation 2	1.28
PASE conformation 3	1.29
Pyrene	0.88

$E_{\text{ad}}^{(\text{conf}-2)}$ ), which is in agreement with the previous study on 1-pyrenebutyric acid.<sup>22</sup> Conformation 1, however, might not always be the most stable structure at a finite temperature due to the flexibility of the molecular structure of PASE. Free from the graphene surface, the BSE part may exhibit a greater vibrational contribution to the free energy in conformation 2 than in conformation 1 at the room temperature. Therefore, there can be a realization of the standing conformation at a finite temperature in a vacuum condition. However, the apparent stabilization for conformation 1 relative to conformation 2 ( $E_{\text{ad}}^{(\text{conf}-1)} - E_{\text{ad}}^{(\text{conf}-2)} = 0.35$  eV) strongly suggests that PASE remains in a straight form lying down on graphene at a reasonable temperature range around the room temperature.

Conformation 1 facilitates the adsorptions of both Py and BSE parts. The adsorption of PASE on graphene is due to two contributions of adsorption energies, *i.e.*, from Py and BSE. However, for the total stabilization of PASE, which contributes more, Py or BSE, is a nontrivial question. In conformation 2, where the Py part is lying flat on and the BSE part is directing away from graphene, the Py part will be major contributor to the entire adsorption of PASE. On the other hand, in conformation 3, where the BSE part is lying down and the Py part is directing away from the graphene surface, the major contributor will not be the Py part but the BSE part. Since the difference in adsorption energies between conformation 2 and 3 was only 0.01 eV, it is not easy to determine whether Py or BSE shows the major adsorption effect.

To further understand the adsorption mechanism of PASE, we intended to estimate the adsorption energy of each part, *i.e.*, Py and BSE, separately. For this purpose, an additional

calculation on adsorption energy of only the Py part  $E_{\text{ad}}^{(\text{Py})}$  was performed (the result is shown in Table 1). We assume that the total adsorption is given by the summation of partial contributions, the Py and BSE parts, treating  $E_{\text{ad}}^{(\text{Py})}$  as the partial contribution from the Py part. In the bent PASE form, there may be a deformation energy contribution. Actually, the total energy difference of isolated PASE between the bent and straight structures was  $\approx 0.003$  eV, which is negligible compared with the energy difference found in Table 1. When the other possible deformation energy contributions are neglected, we can uniquely determine the partial contributions from the Py and BSE parts using the following relations as an approximation:

$$E_{\text{ad}}^{(\text{conf-1})} = E_{\text{ad}}^{(\text{Py})} + E_{\text{ad}}^{(\text{BSE})} \quad (1)$$

$$E_{\text{ad}}^{(\text{conf-2})} = E_{\text{ad}}^{(\text{Py})} + E_{\text{ad}}^{(\text{tiltBSE})} \quad (2)$$

$$E_{\text{ad}}^{(\text{conf-3})} = E_{\text{ad}}^{(\text{tiltPy})} + E_{\text{ad}}^{(\text{BSE})} \quad (3)$$

where  $E_{\text{ad}}^{(\text{BSE})}$ ,  $E_{\text{ad}}^{(\text{tiltBSE})}$ , and  $E_{\text{ad}}^{(\text{tiltPy})}$  denote the adsorption energies of the BSE, tilt BSE, and tilt Py parts, respectively.

From Equation 1, the adsorption energy of the BSE part is determined, where  $E_{\text{ad}}^{(\text{BSE})} = 0.75$  eV. This value is nonnegligible compared with the adsorption energy of the Py part ( $E_{\text{ad}}^{(\text{Py})} = 0.88$  eV). However, the adsorption energy of the Py was greater than that of the BSE part ( $E_{\text{ad}}^{(\text{Py})} > E_{\text{ad}}^{(\text{BSE})}$ ). From Equations 2 and 3, we also obtain the partial contribution by the tilt functional group, where  $E_{\text{ad}}^{(\text{tiltPy})} = 0.54$  eV and  $E_{\text{ad}}^{(\text{tiltBSE})} = 0.40$  eV. Thus, even in a tilt configuration, there can be an adsorption contribution by the Py part, greater than that by the BSE part ( $E_{\text{ad}}^{(\text{tiltPy})} > E_{\text{ad}}^{(\text{tiltBSE})}$ ). Furthermore, the AB stacking of the aromatic molecule of Py on graphene is supported. The optimized structures for both conformations 1 and 2 showed the AB stacking of the aromatic ring on graphene. We conclude that the adsorption effect of the BSE is secondary. This implies that the BSE part has movability whereas the Py part remains adsorbed on graphene.

## Kinetic effect

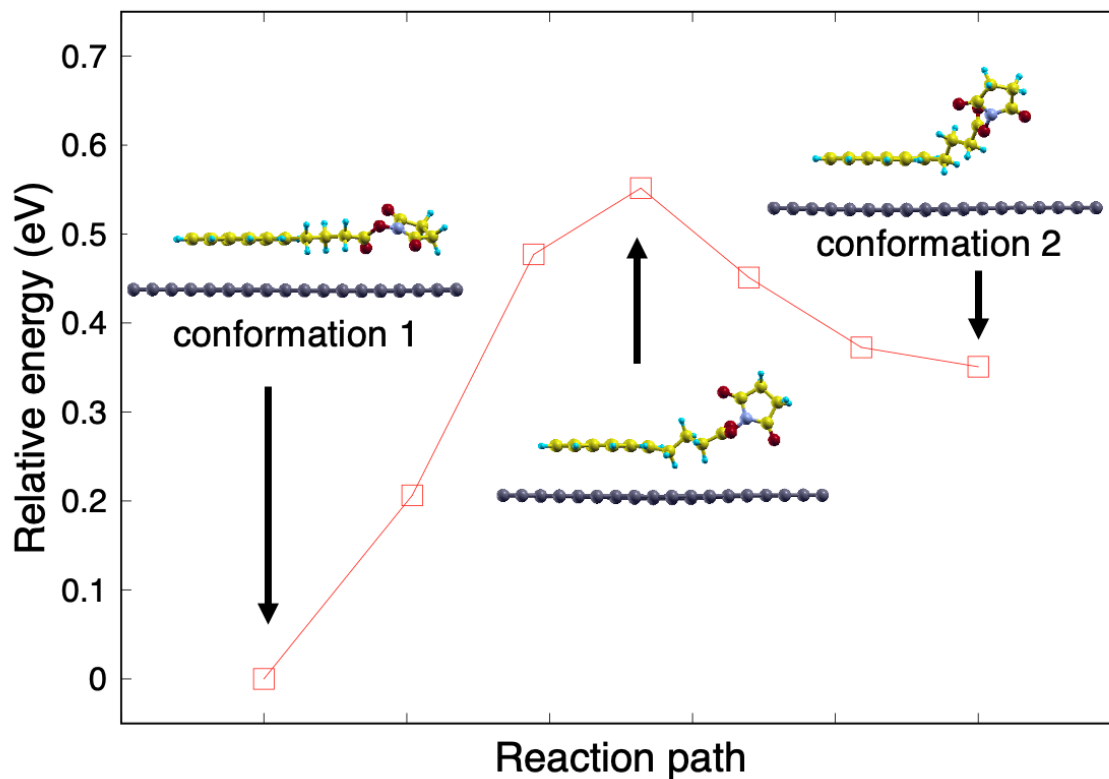


Figure 3: The relative energy of PASE/graphene to the most stable state (conformation 1) using the nudged elastic band method. The first and final images correspond to optimized structures of conformations 1 and 2, respectively.

For the straight PASE structure, it may be difficult to realize both graphene-PASE adsorption and protein-PASE binding simultaneously. For linker activity to catch target protein approaching from various directions, the high conformational flexibility of PASE, *i.e.*, the mobility of the BSE part will be essential. This mobility is determined by the activation energy barrier between conformations 1 and 2. If a high energy barrier exists between conformations 1 and 2, the transition between these two states will not occur, indicating that the PASE structure cannot move back and forth between the bent and straight forms. For confirmation, we calculated the minimum energy pathway corresponding to the standing up process of the BSE part and the activation energy barrier between conformations 1 and



2 by using the nudge elastic band method.<sup>25</sup> The optimized structures of conformations 1 and 2 were used as initial and final images, respectively, and five intermediate configurations were interpolated.

Figure 3 shows the result of the minimum energy pathway. The energy barrier from conformation 1(2) to conformation 2(1) was 0.55(0.20) eV. From this value, the transition between conformations 1 and 2 is possible at around the room temperature. Therefore, the BSE part can change the direction while the Py part remains adsorbed on graphene.

## Effects of the external environment

The details of the PASE structure should depend on the operating environment. Namely, in real operation conditions, solvent molecules exist around linker molecules. Actually, PASE is often used in a solution with water as the solvent. Because the linker is introduced on graphene substrates by drop-casting, PASE is prepared in the water solvent.

Our DFT simulation showed that conformation 1, in which the SI part is lying down, was the most stable. However, the gas-phase environment is assumed in the standard DFT simulation. Notably, PASE is often used in a solution with water, and the solvent may cause change in the adsorption energy via the screening effect. Partly introducing dynamical effect of water solvent in an averaged manner, the change in the dielectric function around PASE adsorbed on graphene may change the relative stability between conformations 1 and 2. To take account of the solvation effect on the PASE on graphene, we adopted DFT combined with 3D-RISM. In this method, the periodic boundary condition is imposed on 3D-RISM as well as on the plane-wave and pseudopotential method.<sup>26</sup> PASE and graphene were explicitly treated by DFT, whereas the solvents around PASE were treated as a continuum distribution of 3D-RISM. We used liquid water as the solvent around the PASE, and the temperature and solvent density were set to 300 K and 1 g/cm<sup>3</sup>, respectively.

The total energy of the conformation 2 relative to the conformation 1 is shown in Table 2, including the result from the standard DFT calculations (the positive value means that

Table 2: The total energies of conformation 2 relative to that of conformation 1 obtained by each calculation.

Model for calculation	Relative energy (eV)
PASE/graphene by DFT	0.35
PASE/graphene by 3D-RISM	0.28
PASE/graphene with two glycines by DFT	0.07
PASE/graphene with three glycines by DFT	0.09

the conformation 1 is energetically more stable than conformation 2). The 3D-RISM calculation showed that the total energy of the conformation 2 relatively approaches that of the conformation 1, compared with the result from the DFT calculations assuming a vacuum condition. This indicates that the standing conformation appears more frequently in the water solvent than in a vacuum.

When the PASE linker is used for biosensing, proteins, such as antibodies, coexist with PASE and graphene substrates. In this situation, amino acids moieties will be near the BSE part on the PASE linker to form an amide bond. Such moieties might sneak in between the BSE part and graphene and block the bending down motion of the BSE part. This motion can cause the BSE part to be raised from the graphene surface. Such an effect can be reproduced by treating molecules directly with DFT. Therefore, we considered including glycine—an amino acid—in the DFT unit cell. The structural optimizations on PASE/graphene with two and three glycine molecules placed near the BSE part were performed.

The total energies of conformation 2 relative to that of conformation 1 are also summarized in Table 2. The relative stabilities of conformation 2 were only within 0.1 eV relative to conformation 1. These results suggest that the existence of amino acids around PASE makes the standing conformation appearing more frequently than in a vacuum condition.

Overall, the trend toward the stabilization for conformation 2 relative to conformation 1 was confirmed from 3D-RISM calculation and calculations on the system containing glycine molecules. Therefore, the external environment around PASE linker is of great importance when we consider the standing up process of the BSE part. Considering the state after the

realization of glycine-PASE binding is future work to further understand the behavior of PASE linkers on graphene substrates. The PASE structure observation using a scanning tunneling microscope or atomic force microscope can also provide us with the key to the conformation problem of linker molecules.

## Conclusions

In this study, the adsorbed structure of 1-pyrenebutanoic acid, succinimidyl ester (PASE) on graphene was investigated with the density functional theory (DFT) calculation. Two locally stable structures—a straight PASE with both the pyrene (Py) and chain-like butanoic acid succinimidyl ester (BSE) parts lying down on graphene (conformation 1) and a bent PASE with the Py part adsorbed on and the BSE part standing up from graphene (conformation 2)—were found. The adsorption energy of conformation 1 was found to be larger than that of conformation 2. The contribution of the BSE part to the adsorption is nonnegligible compared with that of the Py part. However, the adsorption effect of the BSE part was secondary. Considering kinetic effect, the BSE part was found to have mobility at the room temperature.

We also considered effects of the external environment around the PASE linker: changes in the dielectric function around PASE described by 3D-RISM and the behavior of amino acid moieties, such as blocking the bending down motion of the BSE part described by DFT. These external environments were found to contribute to the stabilization of conformation 2 relative to conformation 1. Further calculation on the PASE/graphene system after the realization of glycine-PASE binding, as well as experimental study such as scanning tunneling microscope or atomic force microscope, should be conducted to further clarify the behavior of PASE linker.

## Computational method

The geometrical relaxation was performed on the PASE structure on monolayer graphene using Quantum ESPRESSO.<sup>27-29</sup> A vacuum region of approximately 10 Å in the  $z$ -direction was inserted in our model to prevent spurious interaction between the slabs. A revised Perdew-Burke-Ernzerhof (PBE) functional for a densely packed solid surface (PBEsol),<sup>30</sup> within the generalized gradient approximation (GGA), was used. The ultrasoft pseudopotential<sup>31</sup> was used for each atom to describe electron-ion interaction. To consider the interlayer interaction between the Py group and graphene, at first, we calculated the equilibrium interplanar distance between benzene and graphene by calculating the total energy of the benzene/graphene system for each interplanar distance. The adiabatic-connection fluctuation-dissipation-theorem with random phase approximation including the Hubbard correlation energy (ACFDT-RPA+U),<sup>32</sup> which is considered to accurately reproduce the van der Waals interaction, was employed for comparison. The equilibrium interplanar distance determined by PBEsol was 3.65 Å, whereas ACFDT-RPA+U gave 3.44 Å. By including dispersion correlation of DFT-D3,<sup>33</sup> which is one of the DFT-D approaches,<sup>33-35</sup> the consistency with the result given by ACFDT-RPA+U was confirmed, where the equilibrium interplanar distance was 3.40 Å. The interplanar distance between aromatic ring of PASE and graphene given by PBEsol+D3 ranges from 3.3 to 3.4 Å, which is in agreement with benzene/graphene system. In this study, the structure of PASE/graphene system was investigated by PBEsol+D3. The cutoff was set to 35 and 350 Ry for wave functions and charge density respectively, and  $2 \times 4 \times 1$  Monkhorst-Pack<sup>36</sup>  $\mathbf{k}$ -point was chosen for all calculations. The convergence threshold on forces was  $10^{-6}$  Ry/Bohr. For 3D-RISM, the cutoff energy of the correlation functions was set to 140 Ry, and the Kovalenko and Hirata closure was used.<sup>37</sup>

## Acknowledgement

The authors thank Y. Wicaksono, N. Morisita, S. Akiyama, and R. Ouchi for illuminating discussion and valuable comments. All calculations were done in the computer centers of Kyushu University and ISSP, University of Tokyo.

## References

- (1) Mohanty, N.; Berry, V. Graphene-based single-bacterium resolution biodevice and DNA transistor: interfacing graphene derivatives with nanoscale and microscale biocomponents. *Nano Lett.* **2008**, *8*, 4469–4476.
- (2) Neto, A. C.; Guinea, F.; Peres, N. M.; Novoselov, K. S.; Geim, A. K. The electronic properties of graphene. *Rev. Mod. Phys.* **2009**, *81*, 109.
- (3) Georgakilas, V.; Otyepka, M.; Bourlinos, A. B.; Chandra, V.; Kim, N.; Kemp, K. C.; Hobza, P.; Zboril, R.; Kim, K. S. Functionalization of graphene: covalent and non-covalent approaches, derivatives and applications. *Chem. Rev.* **2012**, *112*, 6156–6214.
- (4) Wang, Y.; Li, Z.; Wang, J.; Li, J.; Lin, Y. Graphene and graphene oxide: biofunctionalization and applications in biotechnology. *Trends Biotechnol.* **2011**, *29*, 205–212.
- (5) Park, S. Y.; Park, J.; Sim, S. H.; Sung, M. G.; Kim, K. S.; Hong, B. H.; Hong, S. Enhanced differentiation of human neural stem cells into neurons on graphene. *Adv. Mater.* **2011**, *23*, H263–H267.
- (6) Myung, S.; Solanki, A.; Kim, C.; Park, J.; Kim, K. S.; Lee, K.-B. Graphene-encapsulated nanoparticle-based biosensor for the selective detection of cancer biomarkers. *Adv. Mater.* **2011**, *23*, 2221–2225.
- (7) Yang, W.; Ratinac, K. R.; Ringer, S. P.; Thordarson, P.; Gooding, J. J.; Braet, F.

- Carbon nanomaterials in biosensors: should you use nanotubes or graphene? *Angew. Chem., Int. Ed.* **2010**, *49*, 2114–2138.
- (8) Geim, A. K.; Novoselov, K. S. The rise of graphene. *Nat. Mater.* **2007**, *6*, 183–191.
- (9) Novoselov, K. S.; Geim, A. K.; Morozov, S. V.; Jiang, D.-e.; Zhang, Y.; Dubonos, S. V.; Grigorieva, I. V.; Firsov, A. A. Electric field effect in atomically thin carbon films. *science* **2004**, *306*, 666–669.
- (10) Loh, K. P.; Bao, Q.; Ang, P. K.; Yang, J. The chemistry of graphene. *J. Mater. Chem.* **2010**, *20*, 2277–2289.
- (11) Chen, R. J.; Zhang, Y.; Wang, D.; Dai, H. Noncovalent sidewall functionalization of single-walled carbon nanotubes for protein immobilization. *J. Am. Chem. Soc.* **2001**, *123*, 3838–3839.
- (12) Kodali, V. K.; Scrimgeour, J.; Kim, S.; Hankinson, J. H.; Carroll, K. M.; De Heer, W. A.; Berger, C.; Curtis, J. E. Nonperturbative chemical modification of graphene for protein micropatterning. *Langmuir* **2011**, *27*, 863–865.
- (13) Liu, J.; Tang, J.; Gooding, J. J. Strategies for chemical modification of graphene and applications of chemically modified graphene. *J. Mater. Chem.* **2012**, *22*, 12435–12452.
- (14) Kokalj, A. XCrySDen—a new program for displaying crystalline structures and electron densities. *J. Mol. Graphics Modell.* **1999**, *17*, 176–179.
- (15) Katz, E. Application of bifunctional reagents for immobilization of proteins on a carbon electrode surface: Oriented immobilization of photosynthetic reaction centers. *J. Electroanal. Chem.* **1994**, *365*, 157–164.
- (16) Jaegfeldt, H.; Kuwana, T.; Johansson, G. Electrochemical stability of catechols with a pyrene side chain strongly adsorbed on graphite electrodes for catalytic oxidation of dihydronicotinamide adenine dinucleotide. *J. Am. Chem. Soc.* **1983**, *105*, 1805–1814.

- (17) Zhou, L.; Mao, H.; Wu, C.; Tang, L.; Wu, Z.; Sun, H.; Zhang, H.; Zhou, H.; Jia, C.; Jin, Q., et al. Label-free graphene biosensor targeting cancer molecules based on non-covalent modification. *Biosens. Bioelectron.* **2017**, *87*, 701–707.
- (18) Wu, G.; Tang, X.; Meyyappan, M.; Lai, K. W. C. Chemical functionalization of graphene with aromatic molecule. 2015 IEEE 15th International Conference on Nanotechnology (IEEE-NANO). 2015; pp 1324–1327.
- (19) Murashima, K.; Murakami, M.; Ogi, H.; Kusakabe, K. CARBON-BASED MATERIAL VIBRATOR, A SENSOR ELEMENT HAVING THE SAME, AND A BIOLOGICAL SUBSTANCE DETECTION DEVICE HAVING THE SAME. U.S. Patent 20210223212, July 22, 2021.
- (20) Haraguchi, T.; Nagakubo, A.; Murashima, K.; Murakami, M.; Ogi, H. Development of 30-GHz phonon biosensor using graphite thin-film resonator. *Proceedings of Symposium on Ultrasonic Electronics* **2021**, *42*, 3Pa2–2.
- (21) Singh, M.; Holzinger, M.; Tabrizian, M.; Winters, S.; Berner, N. C.; Cosnier, S.; Duesberg, G. S. Noncovalently functionalized monolayer graphene for sensitivity enhancement of surface plasmon resonance immunosensors. *J. Am. Chem. Soc.* **2015**, *137*, 2800–2803.
- (22) Bailey, S.; Visontai, D.; Lambert, C. J.; Bryce, M. R.; Frampton, H.; Chappell, D. A study of planar anchor groups for graphene-based single-molecule electronics. *J. Chem. Phys.* **2014**, *140*, 054708.
- (23) Kovalenko, A.; Hirata, F. Three-dimensional density profiles of water in contact with a solute of arbitrary shape: a RISM approach. *Chem. Phys. Lett.* **1998**, *290*, 237–244.
- (24) Sato, H.; Kovalenko, A.; Hirata, F. Self-consistent field, ab initio molecular orbital and three-dimensional reference interaction site model study for solvation effect on carbon monoxide in aqueous solution. *J. Chem. Phys.* **2000**, *112*, 9463–9468.

- (25) Henkelman, G.; Jónsson, H. Improved tangent estimate in the nudged elastic band method for finding minimum energy paths and saddle points. *J. Chem. Phys.* **2000**, *113*, 9978–9985.
- (26) Nishihara, S.; Otani, M. Hybrid solvation models for bulk, interface, and membrane: Reference interaction site methods coupled with density functional theory. *Phys. Rev. B* **2017**, *96*, 115429.
- (27) Giannozzi, P.; Baroni, S.; Bonini, N.; Calandra, M.; Car, R.; Cavazzoni, C.; Ceresoli, D.; Chiarotti, G. L.; Cococcioni, M.; Dabo, I., et al. QUANTUM ESPRESSO: a modular and open-source software project for quantum simulations of materials. *J. Phys.: Condens. Matter* **2009**, *21*, 395502.
- (28) Giannozzi, P.; Andreussi, O.; Brumme, T.; Bunau, O.; Nardelli, M. B.; Calandra, M.; Car, R.; Cavazzoni, C.; Ceresoli, D.; Cococcioni, M., et al. Advanced capabilities for materials modelling with Quantum ESPRESSO. *J. Phys.: Condens. Matter* **2017**, *29*, 465901.
- (29) Giannozzi, P.; Baseggio, O.; Bonfà, P.; Brunato, D.; Car, R.; Carnimeo, I.; Cavazzoni, C.; De Gironcoli, S.; Delugas, P.; Ferrari Ruffino, F., et al. Quantum ESPRESSO toward the exascale. *J. Chem. Phys.* **2020**, *152*, 154105.
- (30) Perdew, J. P.; Ruzsinszky, A.; Csonka, G. I.; Vydrov, O. A.; Scuseria, G. E.; Constantin, L. A.; Zhou, X.; Burke, K. Restoring the density-gradient expansion for exchange in solids and surfaces. *Phys. Rev. Lett.* **2008**, *100*, 136406.
- (31) Vanderbilt, D. Soft self-consistent pseudopotentials in a generalized eigenvalue formalism. *Phys. Rev. B* **1990**, *41*, 7892.
- (32) Kusakabe, K.; Wake, A.; Nagakubo, A.; Murashima, K.; Murakami, M.; Adachi, K.; Ogi, H. Interplanar stiffness in defect-free monocrystalline graphite. *Phys. Rev. Mater.* **2020**, *4*, 043603.



- (33) Grimme, S.; Antony, J.; Ehrlich, S.; Krieg, H. A consistent and accurate ab initio parametrization of density functional dispersion correction (DFT-D) for the 94 elements H-Pu. *J. Chem. Phys.* **2010**, *132*, 154104.
- (34) Grimme, S. Semiempirical GGA-type density functional constructed with a long-range dispersion correction. *J. Comput. Chem.* **2006**, *27*, 1787–1799.
- (35) Grimme, S.; Ehrlich, S.; Goerigk, L. Effect of the damping function in dispersion corrected density functional theory. *J. Comput. Chem.* **2011**, *32*, 1456–1465.
- (36) Monkhorst, H. J.; Pack, J. D. Special points for Brillouin-zone integrations. *Phys. Rev. B* **1976**, *13*, 5188.
- (37) Kovalenko, A.; Hirata, F. Self-consistent description of a metal–water interface by the Kohn–Sham density functional theory and the three-dimensional reference interaction site model. *J. Chem. Phys.* **1999**, *110*, 10095–10112.

# Graphical TOC Entry

